Universiteit
Leiden
The Netherlands

The environmentally-regulated interplay between local three-dimensional chromatin architecture and gene expression

Rashid, F.Z.M.

Citation
Rashid, F. Z. M. (2021, June 22). *The environmentally-regulated interplay between local three-dimensional chromatin architecture and gene expression*. Retrieved from https://hdl.handle.net/1887/3192230

Version:	Publisher's Version
License:	Licence agreement concerning inclusion of doctoral thesis in the Institutional Repository of the University of Leiden
Downloaded from:	https://hdl.handle.net/1887/3192230

Note: To cite this publication please use the final published version (if applicable).

Cover Page

Universiteit Leiden

The handle https://hdl.handle.net/1887/3192230 holds various files of this Leiden University dissertation.

Author: Rashid, F.Z.M.
Title: The environmentally-regulated interplay between local three-dimensional chromatin architecture and gene expression
Issue Date: 2021-06-22

Chapter 4:
HI-NESS: A family of genetically-encoded DNA labels based on a bacterial nucleoid associated protein

Rashid, F-Z.M., Mahlandt, E., Van der Vaart, M., Solari, J., Henneman, B., Brocken, D.J.W., Voskamp, P., Blok, A., Shimizu, T., Meijer, A.H., Goedhart, J., Crémazy, F.G.E., and Dame, R.T. HI-NESS: A family of DNA labelling dyes constructed by fluorescent protein fusion to the DNA binding domain of a bacterial nucleoid associated protein. *Manuscript in preparation*.

Contributions statement:
R.T.D conceived and supervised the project. F.M.R., F.G.E.C., B.H., D.J.W.B, cloned the HI-NESS expression vectors. F.M.R. and M.vd.V performed HI-NESS imaging in *Escherichia coli*. E.M. imaged HI-NESS in eukaryotic cell lines. M.vd.V carried out imaging experiments in zebrafish larvae. F.M.R. analysed imaging data captured for *E. coli*, eukaryotic cell lines, and zebrafish larvae. E.M. analysed imaging data for eukaryotic cell lines. J.S. performed PALM single-particle tracking studies. P.V., A.B., and F.M.R. over-expressed and purified HI-NESS. F.M.R. performed HI-NESS *in vitro* experiments. F.M.R. wrote the manuscript. E.M., M.vd.V, T.S., A.H.M., J.G., F.G.E.C., and R.T.D. edited the manuscript.

Abstract

The interplay between three-dimensional chromosome organisation and genomic processes such as replication and transcription necessitates *in vivo* studies of chromosome dynamics. Fluorescent organic dyes are often used for chromosome labelling *in vivo*. The mode of binding of these dyes to DNA cause its distortion, elongation, and partial unwinding. The structural changes induce DNA damage and interfere with the binding dynamics of chromatin-associated proteins, consequently perturbing gene expression, genome replication, and cell cycle progression. We have developed a minimally-perturbing fluorescent DNA label by translationally fusing a (photo-switchable) fluorescent protein to the DNA binding domain of H-NS – a bacterial nucleoid-associated protein. We show that this DNA label, abbreviated as HI-NESS (H-NS-based indicator for nucleic acid stainings), is minimally-perturbing to genomic processes and labels chromosomes in bacteria, eukaryotic cells in culture, and in zebrafish embryos.

Introduction

Developments in the field of chromosome biology have highlighted an intricate interplay between the spatiotemporal organisation of the chromosome and its activities such as transcription, replication, and segregation (1–3). Investigations of such time-resolved structural dynamics of chromosomes in live cells can be performed by fluorescence microscopy. Fluorescent organic dyes are often the first choice for labelling chromosomes. Bisbenzimides such as 6-diamidino-2-phenylindole (DAPI) and Hoechst insert into the minor groove of A-T rich double-stranded DNA (dsDNA), resulting in an enhanced fluorescence emission in the blue range of the visible spectrum (4–6). Hoechst 33258 has also been conjugated to other fluorescent dyes including, but not limited to, IR-786, fluorescein, and silicon-rhodamine (SiR), that shift its spectral properties from the phototoxic UV/blue range towards longer wavelengths of the spectrum (7–11). Cyanine dyes such as those of the TOTO, TO-PRO, and SYTOX families intercalate between DNA bases and exhibit fluorescence emission enhancement (12–14). The amplified fluorescence of organic dyes upon DNA binding allows DNA labelling with a high signal-to-noise ratio. Due to the reversible binding of the fluorophores to DNA, this feature also allows the detection of single binding events that enables super-resolution imaging by binding-activated localization microscopy (BALM) and fluctuation-assisted BALM (15, 16), and point accumulation for imaging in nanoscale topography (PAINT) (17, 18). Stochastic blinking of fluorophores such as silicon-rhodamine and carboxyrhodamine conjugated to Hoechst allows super-resolution imaging with stimulated emission detection (STED) microscopy (10, 11). Furthermore, bisbenzimides undergo stochastic photoconversion upon UV exposure that shifts the excitation and emission spectra of the dyes from the UV/blue to the blue/green and green/red ranges (19–21). While being problematic for multicolour fluorescence microscopy studies, this property is exploited in single molecule localisation microscopy (SMLM) to image chromatin in intact cell nuclei at a resolution of up to ~40 nm (22, 23).

Despite their broad use, the binding mode of organic DNA labels results in distortion, elongation, and/or partial unwinding of the double-helix (24–27). The structural changes interfere with the binding of DNA processing enzymes and affect their enzymatic activity (28–32). Fluorescent organic dyes can also generate single and double strand breaks in the DNA owing to reactive oxygen species that are produced when the excited fluorophore reacts with molecular oxygen (33, 34). DNA intercalation may also trigger DNA damage signalling and cell cycle arrest in the absence of laser excitation (35). Thus, fluorescent organic DNA dyes are

generally cytotoxic, especially during prolonged incubation periods necessary for time-lapse experiments (35–38). Moreover, some fluorescent organic DNA dyes are unable to permeate the membrane of live cells, requiring cell fixation and the use of permeabilisation agents such as SDS and Triton X-100 for DNA staining. The dyes may strongly bind to RNA as well, calling for RNase A treatment prior to imaging (39).

An alternative approach that relies on covalent labelling of DNA with organic fluorophores has also been introduced. Covalent binding of azide-functionalized fluorophores such as tetramethylrhodamine azide (TAMRA) and Alexa Fluor-azide to alkyne-functionalized nucleotide analogues – EdU (5-ethynyl-20-deoxyuridine) and EdC (5-ethynyl-20-deoxycytidine) – with click chemistry (40) has been used to localize DNA in mammalian cells (41–43), plant tissues (44), and *Escherichia coli* (45–47). While affording resolutions of <20nm with super-resolution microscopy techniques (41, 45), this approach is of limited applicability in live cell imaging. The incorporation of EdU and EdC into DNA triggers DNA damage signalling, interferes with cell cycle progression, and induces apoptosis (48, 49). Fluorescent labelling of the nucleotide analogues requires cell fixation and permeabilisation, and Cu^{+} to catalyse the click reaction (40–47). Moreover, the covalent attachment of large fluorophores to chromosomal DNA would predictably be cytotoxic.

Chromosomes can also be visualised by the expression of fluorescent proteins fused to DNA binding proteins. For eukaryotic systems, the histones H2B, H3 and H4 tagged with (photoactivatable) fluorescent proteins have been shown to incorporate into functional nucleosomes, and to accurately describe chromosome structure throughout the cell cycle (50–52). Such fusions have been used to obtain constitutive DNA staining in mice, nematodes, zebrafish, drosophila and arabidopsis transgenic strains (53–57). mEos2- and mEos3-tagged Heterochromatin protein 1 (HP1) have been used to study the distribution of heterochromatin in human embryonic stem cells at super-resolution (58). In bacterial systems, the distributions of fluorescently labelled nucleoid associated proteins (NAPs) such as GFP-labelled α and β subunits of *E. coli* HU (HupA and HupB, respectively) (59) and Fis (60), and GFP/mCherry-labelled HBsu(61, 62) – the *Bacillus subtilis* homologue of HU — have been shown to overlap with that of DAPI indicating that such protein fusions may be used as alternative DNA labels. Indeed, HupA-mCherry, and GFP-Fis have been used to follow the structural changes to the *E. coli* nucleoid during growth and cell division (63, 64), HupB-

EGFP was used to stain the chromosome in *Mycoplasma smegmatis* to study the distribution of fluorescently-labelled Lsr2 and $Lsr2_{\Delta NTD}$ in single cells (65), and GFP-HBsu has been used to image the nucleoid in *B. subtilis* using 3D-structured illumination microscopy (3D-SIM) to visualise high-density regions in the chromosome (66). However, fluorescent protein fusions to native cell proteins can impair protein function by interfering with protein folding and the equilibria of the protein's interactions with other macromolecules (61, 67–69). Fluorescent protein fusions also require titration of expression levels to match that of the native protein. Furthermore, certain fusions have a limited applicability, for instance, fluorescently labelled histone proteins can only be used to visualise the chromosome in eukaryotic cells.

Collectively, this creates a need for a universal, minimally perturbing DNA label for visualizing chromosomes in live cells. To that end, we have designed a fusion protein that exploits the spectral properties of (photoactivatable) fluorescent proteins, and the DNA binding properties of H-NS – a bacterial nucleoid-associated protein. We show that the DNA label, termed HI-NESS (H-NS-based indicator for nucleic acid stainings), is minimally perturbing to cells, accurately describes chromosome structure in bacteria, eukaryotic cells in culture and live zebrafish, and is customizable with regards to the fluorescent protein used for its visualization.

Materials and methods

Cloning HI-NESS expression vectors

The HI-NESS constructs were assembled and cloned into bacterial pBAD33 and eukaryotic pcDNA3.1(+) expression vectors in a single step using Gibson Assembly (70). The constructs were verified by Sanger sequencing and archived as DH5α glycerol stocks. A complete list of the template plasmids used for Gibson Assembly and the HI-NESS vectors assembled therefrom is provided in Table S4.1. The plasmids designed in this study are deposited on Addgene.

HI-NESS imaging in *Escherichia coli*

E. coli cells (MG1655 and MG1655 Δhns) were grown at 37°C in M9 or H1 medium (71) with the appropriate antibiotics (Table S4.1). The medium was supplemented with 0.1% w/v arabinose (Sigma-Aldrich) to induce expression from the pBAD33 vector. For experiments that required DAPI labelling, the dye (DAPI, Sigma-Aldrich) was added to a final concentration of 10 µg/mL to cultures at an OD_{600} of ~0.1. The cells were harvested at an OD_{600} of 0.2 by centrifugation at 3000 xg for 5 minutes and resuspended in M9 or H1 medium to an OD_{600} of ~2.0. 4.0 µL of the culture was pipetted onto a 1 mm-thick, 1.5% agarose pad prepared on a microscope slide. A cover-slip was placed over the cells and the slide was sealed with nail polish. Extremely clean cover-slips, prepared as described in (72), were used for PALM experiments.

For diffraction-limited imaging, *E. coli* cells were visualised using a Leica TCS SPE or SP8 confocal microscope with a 64X oil immersion objective (NA = 1.4) and excited by 405, 488, or 532 nm laser lines. PALM single particle tracking experiments (73, 74) were carried out using the PALM imaging set-up described in (72) with an exposure time of 15 ms and an inter frame interval of 65 ms. Fluorophores were tracked using the u-track package (75), and the diffusion coefficient of each tracked molecule was calculated using a covariance-based estimator method (76). The tracks were sorted into bound and unbound fractions by fitting a histogram of the diffusion coefficients with the sum of two Gaussian functions. The distribution (mean ± standard deviation) of the unbound molecules was extracted as the apparent diffusion coefficient.

HI-NESS imaging in eukaryotic cell lines: cell culture and sample preparation

HeLa (CCL-2, American Tissue Culture Collection; Manassas, VA, USA) and U-2OS (HTB-96, American Tissue Culture Collection, Manassas, VA, USA) cells were cultured in Dulbecco's modified Eagle's medium + GlutaMAX™-I (Giboc) with

10% fetal calf serum (Giboc) (DMEM + FCS) at 37˚C in 7% CO_2. For transfection 25 000 to 50 000 cells were seeded on 24 mm ø cover-slip (Menzel, Thermo Fisher Scientific) in a 6 well plate with 2 ml DMEM + FCS and cultured for 24 hours. A transfection mix containing 0.5 to 1 µg plasmid (Table S4.1), linear polyethylenimine (PEI, pH 7.3, Polysciences) with a concentration of 1 mg/mL per 100 ng DNA, and 200 µl OptiMEM (Thermo Fisher Scientific) was added to each well. 24 h after transfection, cells were incubated with 2 mM thymidine (CAS: 50-89-5, Sigma-Aldrich) in DMEM + FCS for 18 h to increase the percentage of dividing cells. Thereafter, cells were washed twice with DMEM and incubated for another 5 h before imaging. For SiR-Hoechst labeling, the cells were incubated with 500 nM SiR-DNA (SC007, SpiroChrome Probes for Bioimaging) in DMEM, 4 h prior to imaging. HeLa and U-2OS cells were imaged between 24 to 48 h after transfection in an Attofluor cell chamber (Thermo Fischer Scientific) in 1 ml of Microscopy medium (20 mM HEPES (pH=7.4),137 mM NaCl, 5.4 mM KCl, 1.8 mM $CaCl_2$, 0.8 mM $MgCl_2$ and 20 mM Glucose) at 37˚C.

Blood outgrowth endothelial cells (BOEC) were cultivated from healthy adult donor blood as described previously (77) and cultured in Endothelial Cell Growth Medium-2 BulletKit (CC-3162, Lonza) with 100 U/mL Penicillin (Thermo Fisher Scientific) and 100 µg/mL Streptomycin (Thermo Fisher Scientific), and 20% fetal calf serum (Giboc) (EGM +) at 37˚C in 5% CO_2. Culture dishes and cover-slips were coated with 0.1% gelatin (CAS 9000-70-8, Merck) in phosphate-buffered saline 30 min prior to cell seeding. Transfection was performed with 2 µg endotoxin free plasmid, using the Neon™ Electroporation Transfection system (MPK5000, Invitrogen) with the associated Neon™ Transfection System 100 µl Kit (MPK10096, Invitrogen) generating a single pulse of 1300 V for 30 ms. Cells were seeded on 24 mm ø cover-slip in a 6 well plate with 2 ml EGM +. BOECs were imaged between 24 to 48 h after microporation in an Attofluor cell chamber (Thermo Fischer Scientific) in 1 ml EGM + at 37˚C and 5% CO_2.

HI-NESS imaging in eukaryotic cell lines: spinning disk microscopy

Cells were imaged with a Nikon Ti-E microscope equipped with a Yokogawa CSU X-1 spinning disk unit, a 60x objective (Plan Apo, VC, oil, DIC, NA 1.4), a 100x objective (Apo, TIRF, oil, DIC, N2), Perfect Focus System, and the Nikon NIS elements software. Images were acquired with an Andor iXon 897 CCD camera. mTurquoise2 was imaged using a 440 nm laser line, a triple dichroic mirror (suitable for 440, 514, 561 nm laser) and a 460 – 500 nm emission filter. mEos3.2 was imaged using a 488 nm laser line, a triple dichroic mirror (suitable for 405,

488, 561 nm laser) and a 500 nm long pass emission filter. mEos3.2 was photo-converted with a 405 nm laser line and imaged using 561 nm laser line, a triple dichroic mirror (suitable for 405, 488, 561 nm laser) and a 600 – 660 nm emission filter.

HI-NESS imaging in eukaryotic cell lines: wide-field microscopy

Dividing cells were imaged on a Nikon Ti-E widefield microscope, equipped with a 60x objective (Plan Apo λ, 60x, oil) and a 20x air objective (Plan Apo, VC, DIC, N2), a Lumencor Spectra X light source, the Perfect Focus System, a Hamamatsu C11440-22C camera (SN:100256), and Nikon NIS elements software. For overnight time lapse movies, HeLa cells were imaged in DMEM + FCS at 37˚C and 5% CO_2 in an Attofluor cell chamber (Thermo Fischer Scientific) in a humidified environment. mTurquoise2 was imaged with an excitation wavelength of 440/20 nm and emission light was detected at 459-499 nm with an emission filter in combination with a dichroic mirror (455-491, 523-557, 590-800 nm transmission bands). mScarlet-I was imaged with an excitation wavelength of 550/15 nm and emission light was detected at 570–616 nm with an emission filter in combination with a dichroic mirror (411-452, 485-541, 567-621, 656-793 nm transmission bands). Phase contrast images were acquired with the phase contrast condenser PH3.

HI-NESS imaging in eukaryotic cell lines: confocal microscopy

Confocal microscopy images were obtained with a Leica SP8 equipped with a 63x objective (HC PL Apo, C2S, NA 1.40, oil), the pinhole was set to 1 Airy unit, using line scan, 4x frame averaging, at a scan speed of 40 Hz. SiR-Hoechst was imaged using a 633 nm laser line, emission light was detected between 642 – 788 nm with a HyD detector and the gain was get to 50V. mTurquoise2 was imaged using a 442 nm laser line, emission light was detected between 452 – 598 nm with a HyD detector and the gain was set to 40V. mEos3.2 was imaged using a 488 nm laser line, emission light was detected between 495 – 554 nm with a HyD detector and the gain was set to 110 V.

Line scan analysis

Line scans were performed using the ‘Plot profile’ function in Fiji (78). All profiles were normalized to the most intense pixel of the line scan that was assigned an arbitrary intensity value of 1000.

HI-NESS imaging in zebrafish embryos and larvae

Zebrafish lines used in this study (AB/TL wild types) were handled in compliance with local animal welfare regulations, as overseen by the Animal Welfare Body of Leiden University (License number: 10612) and maintained according to standard protocols (http://zfin.org/). All experiments were done on embryos or larvae up to 5 days post-fertilization (dpf), that had not yet reached the free-feeding stage. Embryos/larvae were kept in egg water (60 μg/ml Instant Ocean sea salts) at 28.5°C and anesthetized with 0.02% ethyl 3-aminobenzoate methanesulfonate (Tricaine, Sigma-Aldrich) before imaging and fixation.

To achieve mosaic expression of HI-NESS and the mEos3.2 control, 25 – 50 pg of pRD188 or pRD190 (Table S4.1) in 1x Danieau buffer (58 mM NaCl, 0.7 mM KCl, 0.4 mM $MgSO_4$, 0.6 mM $Ca(NO_3)_2$ and 5.0 mM HEPES, pH 7.6.) was microinjected into zebrafish embryos at the one-cell stage. After 24 hours, the embryos were screened for fluorescence using a Leica MZ16FA stereo fluorescence microscope. For co-staining with DAPI, larvae expressing HI-NESS or the mEos3.2 control were fixed with 4% PFA in 1x PBS at 4°C overnight. Fixed larvae were washed with 1x PBS and stained with DAPI (Sigma-Aldrich) at a final concentration of 100 μg/ml in 1x PBS. Fixed or live embryos of 2 dpf were mounted with 1.5% low melting point agarose (SERVA) in egg water and imaged using a Leica TCS SPE or SP8 confocal microscope with a 40X water immersion objective (NA = 0.8) and excited by 405, 488, or 532 nm laser lines.

Results and Discussion

HI-NESS can be displaced by native H-NS from chromosomal DNA

We engineered HI-NESS by translationally fusing mEos3.2, a photo-switchable fluorescent protein, to the N-terminus of an *Escherichia coli* H-NS truncation comprising residues 80-137 of the wild-type protein. In this construct, mEos3.2 allows visualisation of the DNA-labelling protein in diffraction-limited and super-resolution microscopy; residues 96-137 of H-NS fold into a DNA-binding domain, and H-NS residues 80-95 form a linker that separates the aforementioned moieties to prevent steric clashes and protein misfolding. In this construct, mEos3.2 was fused to the DNA binding domain of H-NS as opposed to full length H-NS, to achieve a high DNA dissociation constant (79), and to prevent the potential multimerization of HI-NESS that may arise from the presence of an oligomerisation domain (65). These features are expected to make the DNA labelling protein less perturbing to genomic transactions in the cell. To verify this, the distribution of HI-NESS was tested in *E. coli*, where the protein was ectopically expressed from a plasmid. HI-NESS was expected to be outcompeted by native H-NS in binding to chromosomal DNA, while DNA labelling with a high signal-to-noise ratio was expected in the absence of endogenous H-NS. Indeed, HI-NESS distributes relatively homogeneously in wild-type *E. coli* with poor colocalisation with DAPI (Figure 4.1A). In comparison, the distribution of HI-NESS correlates well with the DAPI signal in *E. coli* Δ*hns* (Figure 4.1B).

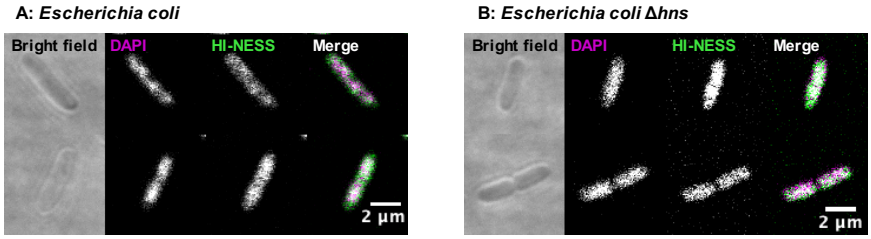

Figure 4.1: HI-NESS distribution in wild-type *Escherichia coli* and *E. coli* Δ*hns*. A: HI-NESS (green) distributes homogeneously in *E. coli* and correlates poorly with the DAPI signal (magenta). **B:** The HI-NESS signal correlates well with the distribution of the DAPI signal in *E. coli* Δ*hns*. A white signal in the Merge images represents colocalization.

To further verify the higher dissociation constant of HI-NESS compared to mEos3.2-H-NS, we used PALM single-particle tracking (73, 74) to characterise the mobility of mEos3.2, HI-NESS, and mEos3.2-H-NS in wild-type *E. coli*. We determined the apparent diffusion coefficients (D_{app}) of these proteins to be 0.44±0.33 µm^2/s (n=1320), 0.31±0.26 µm^2/s (n=3768) and 0.08±0.15 µm^2/s (n=3559), respectively (Figure 4.2). The D_{app} for mEos3.2 in our measurements is an order of magnitude lower than previously reported (74). This is due to longer

camera/laser exposure times and inter frame intervals used in our study. An exposure time of 15 ms in our study – versus 1 ms in (74) – increased the motion blur effect (80) limiting the detection of the population of fast-diffusing mEos3.2 fluorophores. Additionally, our inter frame interval of 65 ms limited the resolution of the sub-diffusive trajectory of the fluorophore in the cytoplasm, hence D_{app} was underestimated (74). Nevertheless, all our single particle tracking experiments were performed with the same imaging parameters ensuring that the D_{app} values determined in our study can be compared.

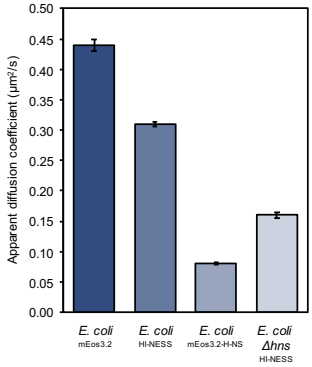

Figure 4.2: Measurements of the apparent diffusion coefficients (D_{app}) of mEos3.2, HI-NESS, and mEos3.2-H-NS with PALM single-particle tracking. mEos3.2 in *E. coli*: D_{app} = 0.44±0.33 μm²/s, n=1320; **HI-NESS in *E. coli*:** D_{app} = 0.31±0.26 μm²/s, n=3768; **mEos3.2-H-NS in *E. coli*:** D_{app} = 0.08±0.15 μm²/s, n=3559; **HI-NESS in *E.coli Δhns*:** D_{app} = 0.16±0.22 μm²/s, n=1796. The errors for D_{app} values in the figure legend are the standard deviations of the apparent diffusion coefficients of the fluorophores and, as such, represent the distribution of diffusion coefficients of unbound fluorescent molecules as determined by PALM single-particle tracking. The errorbars in the graph represent standard error of the mean.

Apparent diffusion coefficients of proteins in the *E. coli* cytoplasm that do not exhibit specific interactions with cytosolic elements, follow the Einstein-Stoke's equation for the diffusion of spherical particles in a classical fluid. Apparent diffusion coefficients are predictable for molecules up to a size of ~110 kDa, with a 30% increase in molecular weight accounting for a 10% decrease in the apparent diffusion coefficient (81). Larger decreases indicate drag due to increased interaction with cytosolic contents (81). HI-NESS (32.1 kDa) has a ~30% lower D_{app} than the fluorophore itself (25.7 kDa). With a molecular weight ~26% larger than that of mEos3.2, the size of HI-NESS only accounts for ~10% of the decrease (81). The difference in D_{app} values may indicate DNA binding by HI-NESS, however, it may also be accounted for by the protein structured as a pair of spheres held together by a flexible linker, rather than an ideal spherical particle. The ~4-fold higher D_{app} of HI-NESS (32.1 kDa) compared to that of mEos3.2-H-NS (41.3 kDa, ~30% larger than HI-NESS) highlights that HI-NESS has a higher

dissociation constant, and may thus be minimally perturbing to genome transactions. Furthermore, in *E. coli* Δ*hns*, HI-NESS has a D_{app} value of 0.16±0.22 $\mu m^2/s$ (n=1796) – ~50% lower than that observed in wild-type *E. coli* (Figure 4.2). This indicates that in wild-type *E. coli*, HI-NESS can be displaced by native H-NS from binding to the chromosome. Together, these results imply that HI-NESS is not a suitable DNA stain for use in *E. coli*.

HI-NESS labels chromosomes in eukaryotic cells

The DNA binding properties of HI-NESS make it an excellent candidate for chromosome labelling in eukaryotic cells. A pcDNA3.1(+) vector was used to express HI-NESS flanked by a pair of SV40 T-antigen derived nuclear localisation signals (NLSs) in HeLa, BOEC, and U2OS cells. The fluorescence signal appeared as several discrete and dense foci in nuclei (Figure 4.3 and S4.1) that overlapped with the SiR-Hoechst signal (Figure 4.3). Such foci were not visible when the cells expressed NLS-mEos3.2-NLS lacking the H-NS DNA binding domain (Figure S4.2). HI-NESS also accumulated in nucleoli – structures that tend to be devoid of DNA, but enriched in RNA and protein (Figure 4.3 and S4.1). The accumulation is expected to be largely non-specific and to occur due to high levels of HI-NESS in the nucleus since HI-NESS lacks detectable nucleolar localisation/retention signals (NoRSs) (82, 83), and the SV40 T-antigen derived NLS cannot drive nucleolar accumulation of proteins (84). However, the affinity of HI-NESS for RNA in *in vitro* assays indicates that the accumulation may partly be due to RNA labelling (Supplementary methods; Table S4.2; Figure S4.3).

We then evaluated the experimental advantage of using HI-NESS over fluorescently tagged histone proteins to label eukaryotic chromosomes. H2A-mTurquoise2 (H2A-mTq2) (85) was expressed in HeLa cells and the nuclei were co-stained with SiR-Hoechst. H2A-mTq2 exhibited extensive nucleolar accumulation that drowned the fluorescence signal over the rest of the nucleus, consequently, reducing the signal-to-noise ratio for chromosome visualisation (Figure 4.4, Nuclei 1&2). Nucleolar accumulation of histones has also been observed for fluorescently-labelled H2B, driven by the presence of a NoRS in the protein's nuclear localisation signal (86). NoRS tend to be enriched in positively-charged (basic) amino acids that facilitate electrostatic interactions with the negatively-charged (acidic) contents of the nucleolus (86). In the case of H2A-mTq2, nucleolar accumulation occurs in the absence of a detectable NoRS in the construct (82, 83), and may be promoted by the inherent basicity of the protein. Occasionally, we observed cells with minimal, if any, nucleolar accumulation of

H2A-mTq2 (Figure 4.4, Nuclei 3&4). These cells expressed low levels of H2A-mTq2 as inferred from low fluorescence in the mTurquoise2 channel. In these cases, line scans across nuclei show that the H2A-mTq2 signal recapitulates the SiR-Hoechst signal (Figure 4.4, Nuclei 3&4). A similar observation was made for nuclei that lacked visible nucleoli (Figure 4.4, Nucleus 5).

We co-expressed HI-NESS and H2A-mTq2 in HeLa cells to compare the distribution of the DNA labels in the same nuclei. The study reproduced the extensive nucleolar accumulation of H2A-mTq2 (Figure 4.5). In comparison, chromosomes were visualised with a high signal-to-noise ratio in the HI-NESS channel, with the DNA label exhibiting decreased nucleolar accumulation (Figure 4.5) compared to cells in which only HI-NESS was ectopically expressed (Figure 4.3). This indicates that H2A-mTq2 has a higher propensity for nucleolar retention than HI-NESS and excludes HI-NESS from the sub-nuclear compartment.

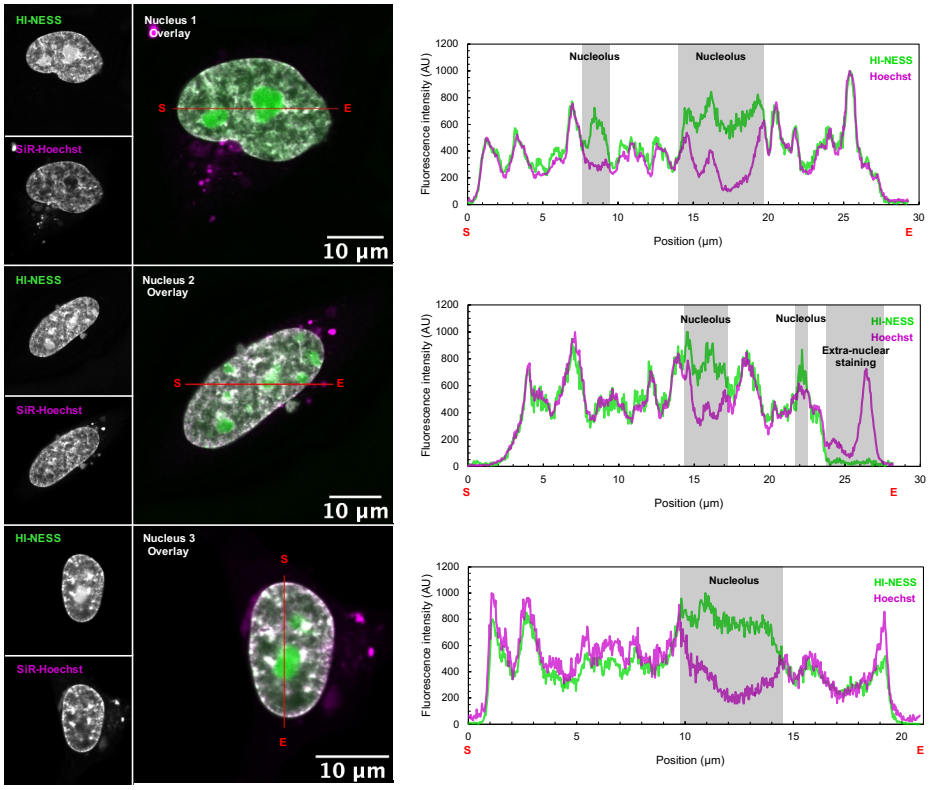

Figure 4.3: HI-NESS labels chromosomes in HeLa cells in culture. Line scans (marked in red with start and end positions indicated with S and E, respectively) across nuclei of HeLa cells co-stained with HI-NESS (green) and SiR-Hoechst (magenta) highlight the overlap between the distributions of the two DNA labels. However, HI-NESS also accumulates in nucleoli due to high levels of the protein in the nucleus and its affinity for RNA as detected in *in vitro* studies (Figure S4.3).

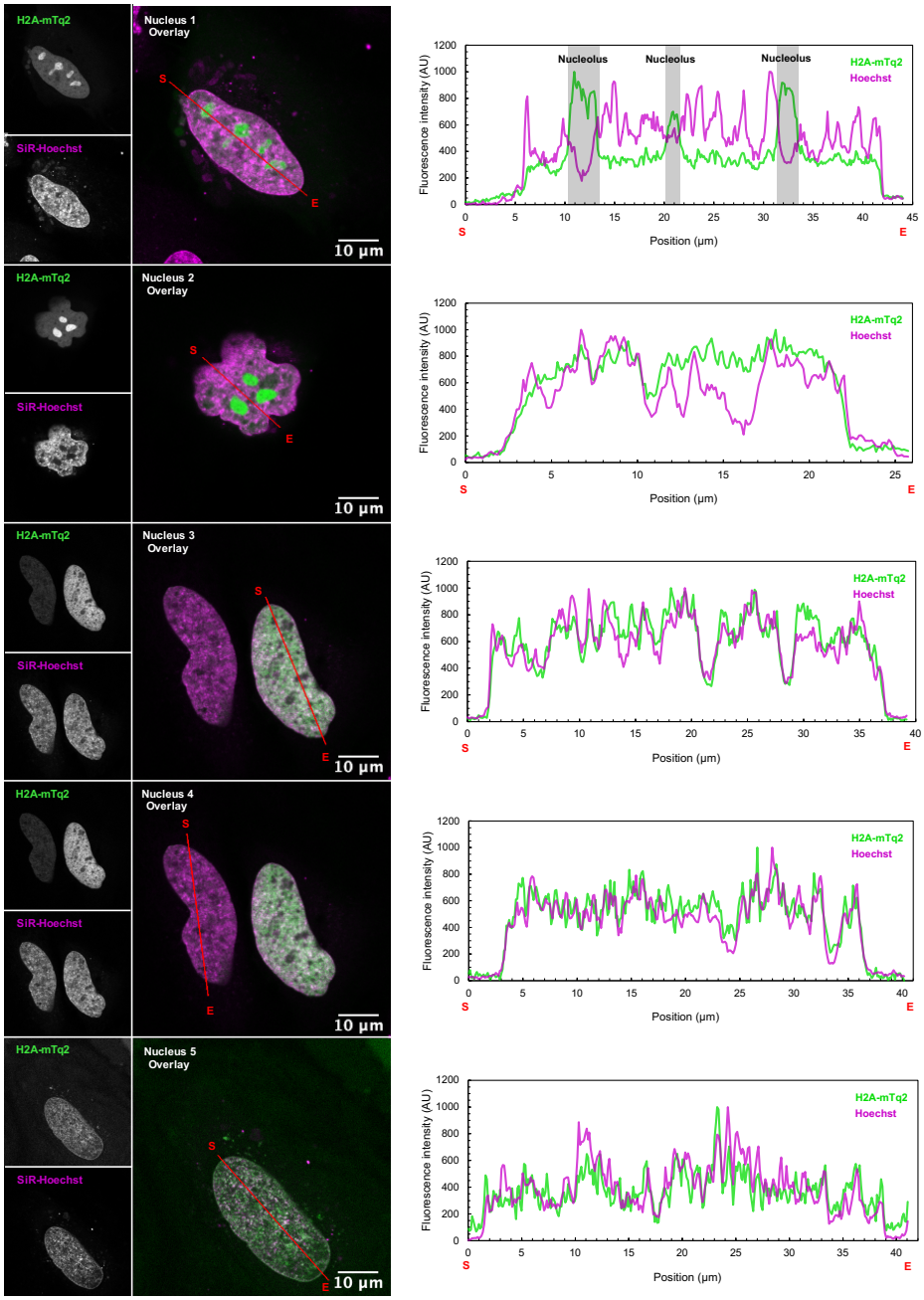

Figure 4.4: The overlap between H2A-mTurquoise2 (green) and SiR-Hoechst (magenta) signals in HeLa cells. Nuclei 1 and 2: Extensive nucleolar accumulation of H2A-mTurquoise2 (H2A-mTq2) drowns its fluorescent signal over the rest of the nucleus. Line scans (marked in red with start and end positions indicated with S and E, respectively) across such nuclei show that the H2A-mTq2 signal only recapitulates that of SiR-Hoechst when the line scan does not cross a nucleolus. **Nuclei 3, 4, and 5:** In cells expressing low levels of H2A-mTq2 (nuclei 3, and 4), and in nuclei with no visible nucleoli (nucleus 5) the distribution of the SiR-Hoechst and H2A-mTq2 signals are comparable.

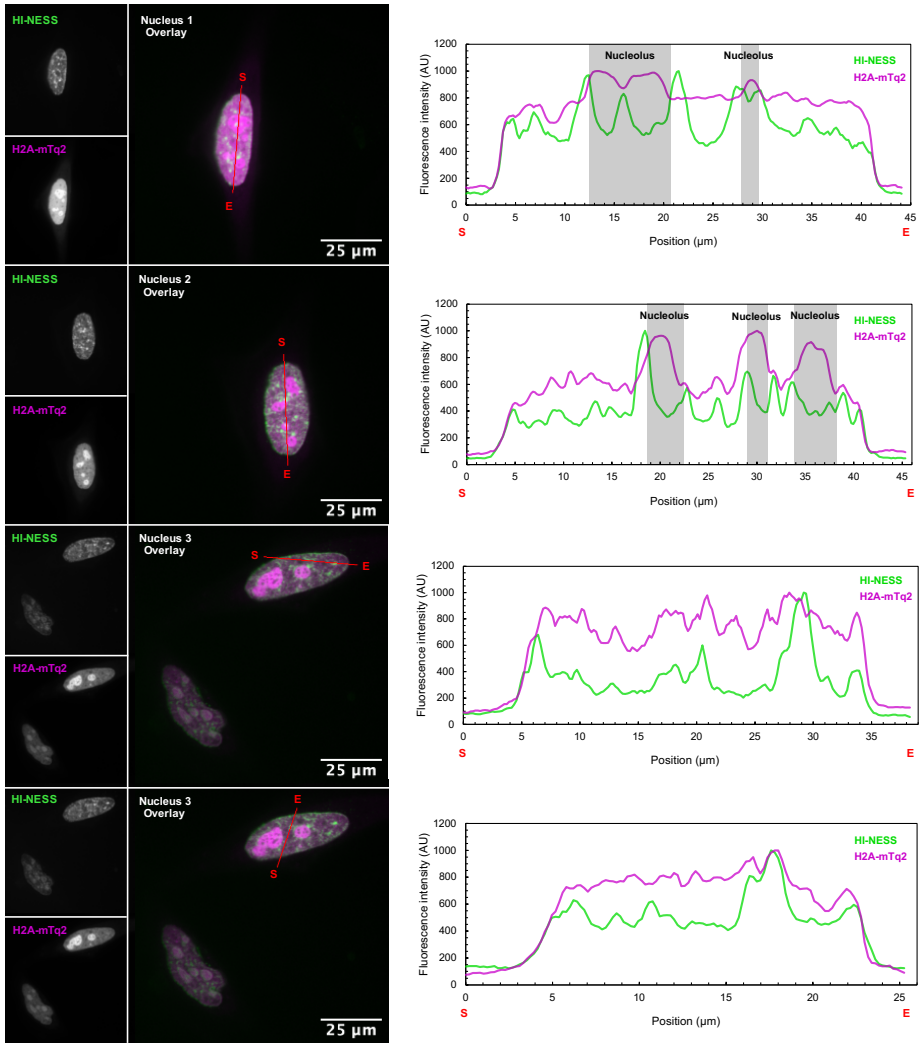

Figure 4.5: HI-NESS (green) labels the chromosomes of HeLa cells in culture with a higher signal-to-noise ratio than H2A-mTq2 (magenta). In HeLa cells co-expressing HI-NESS and H2A-mTq2, the fluorescently-tagged histone exhibits higher nucleolar retention than HI-NESS and, consequently, stains the chromosomes with a lower signal-to-noise ratio. Line scans (marked in red with start and end positions indicated with S and E, respectively) across these nuclei highlight the effect of nucleolar retention on the signal over the rest of the nucleus and show a similarity in the distribution of the DNA labelling proteins in non-nucleolar regions.

HI-NESS as a DNA labelling protein in zebrafish

The feasibility of chromosomal DNA staining in whole organisms using HI-NESS was investigated in zebrafish. HI-NESS and the NLS-mEos3.2-NLS control were expressed in zebrafish from pcDNA3.1(+) vectors microinjected into the embryos at the 1-cell stage. The distribution of the fluorophores was visualised using confocal laser scanning microscopy in fixed zebrafish larvae co-stained with DAPI.

Predictably, HI-NESS was detected in cell nuclei where its distribution overlapped with that of DAPI (Figure 4.6, Movies S4.1-S4.5). Interestingly, nucleolar accumulation of HI-NESS was not observed. This may be due to a lower expression of HI-NESS, however, it also indicates that while HI-NESS may exhibit a comparable affinity for RNA and DNA *in vitro* (Figure S4.3), HI-NESS preferentially binds to DNA in an *in vivo* system. In zebrafish larvae expressing NLS-mEos3.2-NLS lacking the H-NS DNA binding domain, the fluorescent protein accumulated in nucleoli and distributed uniformly over the non-nucleolar regions of the nucleus. Evidently, the mEos3.2 signal did not recapitulate the distribution of DAPI (Figure S4.4, Movies S4.6-S4.8).

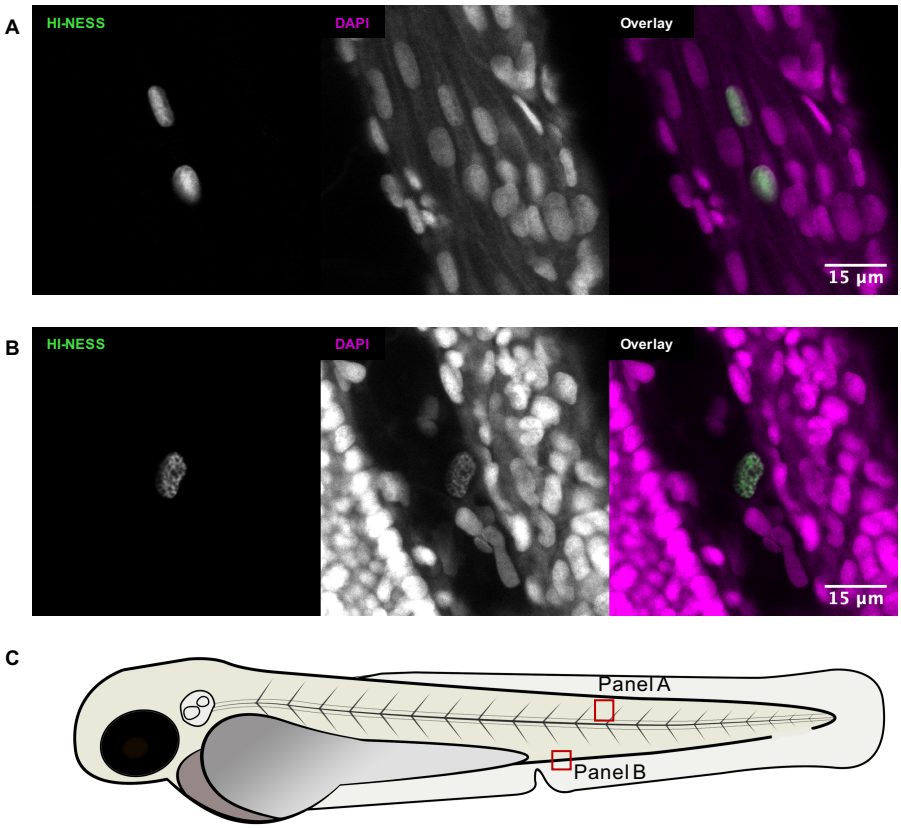

Figure 4.6: HI-NESS labels chromosomes in zebrafish larvae. The distribution of the mEos3.2 signal (green) in nuclei of zebrafish larvae overlapped with that of DAPI (magenta). Nucleolar accumulation of HI-NESS was not observed. **A:** Striated muscle cells (Trunk); **B:** from left to right: trunk, blood vessel, yolk extension. The HI-NESS labelled cell is within a blood vessel. The approximate locations in the zebrafish embryo at which **A** and **B** were imaged is provided in **C**.

Zebrafish larvae exhibited a mosaic expression of HI-NESS and NLS-mEos3.2-NLS in our experiments (Figure S4.5) owing to the microinjection of the pcDNA3.1(+)

vector into embryos at the one-cell stage. For constitutive HI-NESS expression in an animal model, the Tol2 transposon-based gene insertion system (reviewed in (87, 88)) may be used to integrate the HI-NESS gene into the genome. Constructs with the HI-NESS gene placed downstream of a cell-type-specific promoter may also be designed to selectively label nuclei in a live animal model.

HI-NESS is customisable

HI-NESS is a modular protein comprised of fluorescent, DNA-binding, and, optionally, organelle-targeting segments. The protein domains forming these segments can potentially be switched out for others exhibiting similar properties. We have generated a range of HI-NESS labels where mEos3.2 has been swapped for non-photoswitchable fluorescent proteins (Table S4.1). In eukaryotes, HI-NESS can be used to visualise chromosome dynamics during the cell cycle at a high spatial and temporal resolution (Movie S4.9), and follow the movements of nuclei in a live animal model (Movie S4.10). The addition of organelle-targeting/localisation signals can be exploited to specifically label nuclear, mitochondrial, or chloroplast DNA. In prokaryotes, we predict that HI-NESS can be used to visualise the chromosome in bacteria naturally lacking H-NS and H-NS-like proteins. The H-NS-based DNA-binding module can also be replaced with archaeal DNA-binding domains or stable variants evolved from the H-NS-based module to study chromosome dynamics in extremophiles.

Conclusion

We have designed a minimally-perturbing, DNA label to visualise chromosomes in bacteria, eukaryotic cells in culture, and in live animal models. We have shown that in these systems, the distribution of the label (HI-NESS) overlaps with that of traditional DNA labels such as DAPI and SiR-Hoechst. In eukaryotes, HI-NESS offers an alternative to fluorescently labelled histone proteins that tend to accumulate in nucleoli. Furthermore, HI-NESS staining closely mimics that of organic DNA dyes. It is, therefore, a more effective choice for eukaryotic DNA labelling than histone markers.

Availability

Fiji/ImageJ are an open source image processing programs made available by the National Institutes of Health (NIH), Bethesda, USA.

Prism8 is an analysis and graphing software developed by GraphPad Software, San Diego, USA.

References:

1. Dame,R.T., Rashid,F.Z.M. and Grainger,D.C. (2020) Chromosome organization in bacteria: mechanistic insights into genome structure and function. *Nat. Rev. Genet.*, **21**, 227–242.
2. Dame,R.T. and Tark-Dame,M. (2016) Bacterial chromatin: Converging views at different scales. *Curr. Opin. Cell Biol.*, 10.1016/j.ceb.2016.02.015.
3. Yu,M. and Ren,B. (2017) The Three-Dimensional Organization of Mammalian Genomes. *Annu. Rev. Cell Dev. Biol.*, 10.1146/annurev-cellbio-100616-060531.
4. Banerjee,D. and Pal,S.K. (2008) Dynamics in the DNA recognition by DAPI: Exploration of the various binding modes. *J. Phys. Chem. B*, 10.1021/jp077090f.
5. Trotta,E., D'Ambrosio,E., Ravagnan,G. and Paci,M. (1996) Simultaneous and different binding mechanisms of 4',6-diamidino-2- phenylindole to DNA hexamer (d(CGATCG))2: A 1H NMR study. *J. Biol. Chem.*, 10.1074/jbc.271.44.27608.
6. Bailly,C., Colson,P., Hénichart,J. pierre and Houssier,C. (1993) The different binding modes of hoechst 33258 to DNA studied by electirc linear dichroism. *Nucleic Acids Res.*, 10.1093/nar/21.16.3705.
7. Nakayama,A., Bianco,A.C., Zhang,C.Y., Lowell,B.B. and Frangioni,J. V. (2003) Quantification of brown adipose tissue perfusion in transgenic mice using near-infrared fluorescence imaging. *Mol. Imaging*, 10.1162/153535003765276273.
8. Nakamura,A., Takigawa,K., Kurishita,Y., Kuwata,K., Ishida,M., Shimoda,Y., Hamachi,I. and Tsukiji,S. (2014) Hoechst tagging: A modular strategy to design synthetic fluorescent probes for live-cell nucleus imaging. *Chem. Commun.*, 10.1039/c4cc01753f.
9. Dasari,M., Lee,S., Sy,J., Kim,D., Lee,S., Brown,M., Davis,M. and Murthy,N. (2010) Hoechst-IR: An imaging agent that detects necrotic tissue in vivo by binding extracellular DNA. *Org. Lett.*, 10.1021/ol100923d.
10. Lukinavičius,G., Blaukopf,C., Pershagen,E., Schena,A., Reymond,L., Derivery,E., Gonzalez-Gaitan,M., D'Este,E., Hell,S.W., Gerlich,D.W., *et al.* (2015) SiR-Hoechst is a far-red DNA stain for live-cell nanoscopy. *Nat. Commun.*, 10.1038/ncomms9497.
11. Bucevičius,J., Keller-Findeisen,J., Gilat,T., Hell,S.W. and Lukinavičius,G. (2019) Rhodamine-Hoechst positional isomers for highly efficient staining of heterochromatin. *Chem. Sci.*, 10.1039/c8sc05082a.
12. Rye,H.S., Yue,S., Wemmer,D.E., Quesada,M.A., Haugland,R.P., Mathies,R.A. and Glazer,A.N. (1992) Stable fluorescent complexes of double-stranded DNA with bis-intercalating asymmetric cyanine dyes: Properties and applications. *Nucleic Acids Res.*, 10.1093/nar/20.11.2803.
13. Van Hooijdonk,C.A.E.M., Glade,C.P. and Van Erp,P.E.J. (1994) TO-PRO-3 iodide: A novel HeNe laser-excitable DNA stain as an alternative for propidium iodide in multiparameter flow cytometry. *Cytometry*, 10.1002/cyto.990170212.
14. Glazer,A.N. and Rye,H.S. (1992) Stable dye-DNA intercalation complexes as reagents for high-sensitivity fluorescence detection. *Nature*, 10.1038/359859a0.
15. Schoen,I., Ries,J., Klotzsch,E., Ewers,H. and Vogel,V. (2011) Binding-activated localization microscopy of DNA l. *Nano Lett.*, 10.1021/nl2025954.
16. Szczurek,A., Klewes,L., Xing,J., Gourram,A., Birk,U., Knecht,H., Dobrucki,J.W., Mai,S. and Cremer,C. (2017) Imaging chromatin nanostructure with binding-activated localization microscopy based on DNA structure fluctuations. *Nucleic Acids Res.*, 10.1093/nar/gkw1301.
17. Legant,W.R., Shao,L., Grimm,J.B., Brown,T.A., Milkie,D.E., Avants,B.B., Lavis,L.D. and Betzig,E. (2016) High-density three-dimensional localization microscopy across large volumes. *Nat. Methods*, 10.1038/nmeth.3797.
18. Spahn,C.K., Glaesmann,M., Grimm,J.B., Ayala,A.X., Lavis,L.D. and Heilemann,M. (2018) A toolbox for multiplexed super-resolution imaging of the E. coli nucleoid and membrane using novel PAINT labels. *Sci. Rep.*, 10.1038/s41598-018-33052-3.
19. Karg,T.J. and Golic,K.G. (2018) Photoconversion of DAPI and Hoechst dyes to green and red-emitting forms after exposure to UV excitation. *Chromosoma*, 10.1007/s00412-017-0654-5.
20. Zurek-Biesiada,D., Kedracka-Krok,S. and Dobrucki,J.W. (2013) UV-activated conversion of Hoechst 33258, DAPI, and Vybrant DyeCycle fluorescent dyes into blue-excited, green-emitting protonated forms. *Cytom. Part A*, 10.1002/cyto.a.22260.
21. Piterburg,M., Panet,H. and Weiss,A. (2012) Photoconversion of DAPI following UV or violet excitation can cause DAPI to fluoresce with blue or cyan excitation. *J. Microsc.*, 10.1111/j.1365-2818.2011.03591.x.

22. Szczurek,A.T., Prakash,K., Lee,H.K., Zurek-Biesiada,D.J., Best,G., Hagmann,M., Dobrucki,J.W., Cremer,C. and Birk,U. (2014) Single molecule localization microscopy of the distribution of chromatin using hoechst and DAPI fluorescent probes. *Nucl. (United States)*, 10.4161/nucl.29564.
23. Zurek-Biesiada,D., Szczurek,A.T., Prakash,K., Best,G., Mohana,G.K., Lee,H.K., Roignant,J.Y., Dobrucki,J.W., Cremer,C. and Birk,U. (2016) Quantitative super-resolution localization microscopy of DNA in situ using Vybrant® DyeCycle™ Violet fluorescent probe. *Data Br.*, 10.1016/j.dib.2016.01.041.
24. Spielmann,H.P. (1998) Dynamics of a bis-intercalator DNA complex by 1H-detected natural abundance 13C NMR spectroscopy. *Biochemistry*, 10.1021/bi980789e.
25. Spielmann,H.P., Wemmer,D.E. and Jacobsen,J.P. (1995) Solution Structure of a DNA Complex with the Fluorescent Bis-Intercalator TOTO Determined by NMR Spectroscopy. *Biochemistry*, 10.1021/bi00027a004.
26. Kamitori,S. and Takusagawa,F. (1992) Crystal structure of the 2:1 complex between d(GAAGCTTC) and the anticancer drug actinomycin D. *J. Mol. Biol.*, 10.1016/0022-2836(92)90931-9.
27. Günther,K., Mertig,M. and Seidel,R. (2010) Mechanical and structural properties of YOYO-1 complexed DNA. *Nucleic Acids Res.*, 10.1093/nar/gkq434.
28. Chiang,S.Y., Welch,J., Beerman,T.A. and Rauscher,F.J. (1994) Effects of Minor Groove Binding Drugs on the Interaction of TATA Box Binding Protein and TFIIA with DNA. *Biochemistry*, 10.1021/bi00189a003.
29. Störl,K., Störl,J., Zimmer,C. and Lown,J.W. (1993) Minor-groove binders are inhibitors of the catalytic activity of DNA gyrases. *FEBS Lett.*, 10.1016/0014-5793(93)81513-Y.
30. Straney,D.C. and Crothers,D.M. (1987) Effect of Drug–DNA Interactions upon Transcription Initiation at the lac Promoter. *Biochemistry*, 10.1021/bi00381a031.
31. Woynarowski,J.M., McHugh,M., Sigmund,R.D. and Beerman,T.A. (1989) Modulation of topoisomerase II catalytic activity by DNA minor groove binding agents distamycin, Hoechst 33258, and 4',6-diamidine-2-phenylindole. *Mol. Pharmacol.*
32. Parolin,C., Montecucco,A., Ciarrocchi,G., Pedrali-Noy,G., Valisena,S., Palumbo,M. and Palu,G. (1990) The effect of the minor groove binding agent DAPI (2-amidino-diphenyl-indole) on DNA-directed enzymes: an attempt to explain inhibition of plasmid expression in Escherichia coli. *FEMS Microbiol. Lett.*, 10.1016/S0378-1097(05)80065-5.
33. Åkerman,B. and Tuite,E. (1996) Single- and double-strand photocleavage of DNA by YO, YOYO and TOTO. *Nucleic Acids Res.*, 10.1093/nar/24.6.1080.
34. Tycon,M.A., Dial,C.F., Faison,K., Melvin,W. and Fecko,C.J. (2012) Quantification of dye-mediated photodamage during single-molecule DNA imaging. *Anal. Biochem.*, 10.1016/j.ab.2012.03.021.
35. Sen,O., Saurin,A.T. and Higgins,J.M.G. (2018) The live cell DNA stain SiR-Hoechst induces DNA damage responses and impairs cell cycle progression. *Sci. Rep.*, 10.1038/s41598-018-26307-6.
36. Bielawski,K., Woczyski,S. and Bielawska,A. (2001) DNA-binding activity and cytotoxicity of the extended diphenylfuran bisamidines in breast cancer MCF-7 cells. *Biol. Pharm. Bull.*, 10.1248/bpb.24.704.
37. Durand,R.E. and Olive,P.L. (1982) Cytotoxicity, mutagenicity and DNA damage by Hoechst 33342. *J. Histochem. Cytochem.*, 10.1177/30.2.7061816.
38. Haraguchi,T., Ding,D.Q., Yamamoto,A., Kaneda,T., Koujin,T. and Hiraoka,Y. (1999) Multiple-color fluorescence imaging of chromosomes and microtubules in living cells. In *Cell Structure and Function*.
39. Martin,R.M., Leonhardt,H. and Cardoso,M.C. (2005) DNA labeling in living cells. *Cytom. Part A*, 10.1002/cyto.a.20172.
40. Kolb,H.C., Finn,M.G. and Sharpless,K.B. (2001) Click Chemistry: Diverse Chemical Function from a Few Good Reactions. *Angew. Chemie Int. Ed.*, 10.1002/1521-3773(20010601)40:11<2004::aid-anie2004>3.3.co;2-x.
41. Zessin,P.J.M., Finan,K. and Heilemann,M. (2012) Super-resolution fluorescence imaging of chromosomal DNA. *J. Struct. Biol.*, 10.1016/j.jsb.2011.12.015.
42. Salic,A. and Mitchison,T.J. (2008) A chemical method for fast and sensitive detection of DNA synthesis in vivo. *Proc. Natl. Acad. Sci. U. S. A.*, 10.1073/pnas.0712168105.
43. Qu,D., Wang,G., Wang,Z., Zhou,L., Chi,W., Cong,S., Ren,X., Liang,P. and Zhang,B. (2011) 5-Ethynyl-20-deoxycytidine as a new agent for DNA labeling: Detection of proliferating cells. *Anal.*

Biochem., 10.1016/j.ab.2011.05.037.
44. Kotogány,E., Dudits,D., Horváth,G. V. and Ayaydin,F. (2010) A rapid and robust assay for detection of S-phase cell cycle progression in plant cells and tissues by using ethynyl deoxyuridine. *Plant Methods*, 10.1186/1746-4811-6-5.
45. Spahn,C., Endesfelder,U. and Heilemann,M. (2014) Super-resolution imaging of Escherichia coli nucleoids reveals highly structured and asymmetric segregation during fast growth. *J. Struct. Biol.*, 10.1016/j.jsb.2014.01.007.
46. Spahn,C., Cella-Zannacchi,F., Endesfelder,U. and Heilemann,M. (2015) Correlative super-resolution imaging of RNA polymerase distribution and dynamics, bacterial membrane and chromosomal structure in Escherichia coli. *Methods Appl. Fluoresc.*, 10.1088/2050-6120/3/1/014005.
47. Ferullo,D.J., Cooper,D.L., Moore,H.R. and Lovett,S.T. (2009) Cell cycle synchronization of Escherichia coli using the stringent response, with fluorescence labeling assays for DNA content and replication. *Methods*, 10.1016/j.ymeth.2009.02.010.
48. Zhao,H., Halicka,H.D., Li,J., Biela,E., Berniak,K., Dobrucki,J. and Darzynkiewicz,Z. (2013) DNA damage signaling, impairment of cell cycle progression, and apoptosis triggered by 5-ethynyl-2′-deoxyuridine incorporated into DNA. *Cytom. Part A*, 10.1002/cyto.a.22396.
49. Ligasová,A., Liboska,R., Friedecký,D., Mičová,K., Adam,T., Ozdian,T., Rosenberg,I. and Koberna,K. (2016) Dr Jekyll and Mr Hyde: A strange case of 5-ethynyl-2′-deoxyuridine and 5-ethynyl-2′-deoxycytidine. *Open Biol.*, 10.1098/rsob.150172.
50. Kanda,T., Sullivan,K.F. and Wahl,G.M. (1998) Histone-GFP fusion protein enables sensitive analysis of chromosome dynamics in living mammalian cells. *Curr. Biol.*, 10.1016/S0960-9822(98)70156-3.
51. Kimura,H. and Cook,P.R. (2001) Kinetics of core histones in living human cells: Little exchange of H3 and H4 and some rapid exchange of H2B. *J. Cell Biol.*, 10.1083/jcb.153.7.1341.
52. McKinney,S.A., Murphy,C.S., Hazelwood,K.L., Davidson,M.W. and Looger,L.L. (2009) A bright and photostable photoconvertible fluorescent protein. *Nat. Methods*, 10.1038/nmeth.1296.
53. Köster,R.W. and Fraser,S.E. (2001) Tracing transgene expression in living zebrafish embryos. *Dev. Biol.*, 10.1006/dbio.2001.0242.
54. Fraser,S.T., Hadjantonakis,A.K., Sahr,K.E., Willey,S., Kelly,O.G., Jones,E.A.V., Dickinson,M.E. and Baron,M.H. (2005) Using a histone yellow fluorescent protein fusion for tagging and tracking endothelial cells in ES cells and mice. *Genesis*, 10.1002/gene.20139.
55. Das,T., Payer,B., Cayouette,M. and Harris,W.A. (2003) In vivo time-lapse imaging of cell divisions during neurogenesis in the developing zebrafish retina. *Neuron*, 10.1016/S0896-6273(03)00066-7.
56. Savoian,M.S. and Rieder,C.L. (2002) Mitosis in primary cultures of Drosophila melanogaster larval neuroblasts. *J. Cell Sci.*
57. Boisnard-Lorig,C., Colon-Carmona,A., Bauch,M., Hodge,S., Doerner,P., Bancharel,E., Dumas,C., Haseloff,J. and Berger,F. (2001) Dynamic analyses of the expression of the histone::YFP fusion protein in Arabidopsis show that syncytial endosperm is divided in mitotic domains. *Plant Cell*, 10.1105/tpc.13.3.495.
58. Hu,Y.S., Zhu,Q., Elkins,K., Tse,K., Li,Y., Fitzpatrick,J.A.J., Verma,I.M. and Cang,H. (2013) Light-sheet Bayesian microscopy enables deepcell super-resolution imaging of heterochromatin in live human embryonic stem cells. *Opt. Nanoscopy*, 10.1186/2192-2853-2-7.
59. Wery,M., Woldringh,C.L. and Rouviere-Yaniv,J. (2001) HU-GFP and DAPI co-localize on the Escherichia coli nucleoid. *Biochimie*, 10.1016/S0300-9084(01)01254-8.
60. Hadizadeh,N., Johnson,R.C. and Marko,J.F. (2016) Facilitated dissociation of a nucleoid protein from the bacterial chromosome. *J. Bacteriol.*, 10.1128/JB.00225-16.
61. Köhler,P. and Marahiel,M.A. (1997) Association of the histone-like protein HBsu with the nucleoid of Bacillus subtilis. *J. Bacteriol.*, 10.1128/jb.179.6.2060-2064.1997.
62. Smits,W.K. and Grossman,A.D. (2010) The transcriptional regulator Rok binds A+T-rich DNA and is involved in repression of a mobile genetic element in Bacillus subtilis. *PLoS Genet.*, 10.1371/journal.pgen.1001207.
63. Hadizadeh Yazdi,N., Guet,C.C., Johnson,R.C. and Marko,J.F. (2012) Variation of the folding and dynamics of the Escherichia coli chromosome with growth conditions. *Mol. Microbiol.*, 10.1111/mmi.12071.
64. Fisher,J.K., Bourniquel,A., Witz,G., Weiner,B., Prentiss,M. and Kleckner,N. (2013) Four-

dimensional imaging of E. coli nucleoid organization and dynamics in living cells. *Cell*, 10.1016/j.cell.2013.04.006.
65. Kołodziej,M., Trojanowski,D., Bury,K., Hołówka,J., Paściak,M., Matysik,W., Kąkolewska,H., Feddersen,H., Giacomelli,G., Bramkamp,M., *et al.* (2020) Lsr2 is a nucleoid-associated protein that exerts pleiotropic effects on mycobacterial cellular processes. *bioRxiv*, 10.1101/2020.04.27.063487.
66. Marbouty,M., Le Gall,A., Cattoni,D.I., Cournac,A., Koh,A., Fiche,J.B., Mozziconacci,J., Murray,H., Koszul,R. and Nollmann,M. (2015) Condensin- and Replication-Mediated Bacterial Chromosome Folding and Origin Condensation Revealed by Hi-C and Super-resolution Imaging. *Mol. Cell*, 10.1016/j.molcel.2015.07.020.
67. Heo,M., Nord,A.L., Chamousset,D., Van Rijn,E., Beaumont,H.J.E. and Pedaci,F. (2017) Impact of fluorescent protein fusions on the bacterial flagellar motor. *Sci. Rep.*, 10.1038/s41598-017-11241-w.
68. Zhang,F., Moniz,H.A., Walcott,B., Moremen,K.W., Wang,L. and Linhardt,R.J. (2014) Probing the impact of GFP tagging on Robo1-heparin interaction. *Glycoconj. J.*, 10.1007/s10719-014-9522-1.
69. Swulius,M.T. and Jensen,G.J. (2012) The helical mreb cytoskeleton in Escherichia coli MC1000/pLE7 is an artifact of the N-terminal yellow fluorescent protein tag. *J. Bacteriol.*, 10.1128/JB.00505-12.
70. Gibson,D.G., Young,L., Chuang,R.Y., Venter,J.C., Hutchison,C.A. and Smith,H.O. (2009) Enzymatic assembly of DNA molecules up to several hundred kilobases. *Nat. Methods*, 10.1038/nmeth.1318.
71. Hazelbauer,G.L., Mesibov,R.E. and Adler,J. (1969) Escherichia coli mutants defective in chemotaxis toward specific chemicals. *Proc. Natl. Acad. Sci. U. S. A.*, 10.1073/pnas.64.4.1300.
72. Solari,J., Anquez,F., Scherer,K.M. and Shimizu,T.S. (2018) Bacterial chemoreceptor imaging at high spatiotemporal resolution using photoconvertible fluorescent proteins. In *Methods in Molecular Biology*.
73. Manley,S., Gillette,J.M., Patterson,G.H., Shroff,H., Hess,H.F., Betzig,E. and Lippincott-Schwartz,J. (2008) High-density mapping of single-molecule trajectories with photoactivated localization microscopy. *Nat. Methods*, 10.1038/nmeth.1176.
74. English,B.P., Hauryliuk,V., Sanamrad,A., Tankov,S., Dekker,N.H. and Elf,J. (2011) Single-molecule investigations of the stringent response machinery in living bacterial cells. *Proc. Natl. Acad. Sci. U. S. A.*, 10.1073/pnas.1102255108.
75. Jaqaman,K., Loerke,D., Mettlen,M., Kuwata,H., Grinstein,S., Schmid,S.L. and Danuser,G. (2008) Robust single-particle tracking in live-cell time-lapse sequences. *Nat. Methods*, 10.1038/nmeth.1237.
76. Vestergaard,C.L., Blainey,P.C. and Flyvbjerg,H. (2014) Optimal estimation of diffusion coefficients from single-particle trajectories. *Phys. Rev. E - Stat. Nonlinear, Soft Matter Phys.*, 10.1103/PhysRevE.89.022726.
77. Martin-Ramirez,J., Hofman,M., Van Den Biggelaar,M., Hebbel,R.P. and Voorberg,J. (2012) Establishment of outgrowth endothelial cells from peripheral blood. *Nat. Protoc.*, 10.1038/nprot.2012.093.
78. Schindelin,J., Arganda-Carreras,I., Frise,E., Kaynig,V., Longair,M., Pietzsch,T., Preibisch,S., Rueden,C., Saalfeld,S., Schmid,B., *et al.* (2012) Fiji: An open-source platform for biological-image analysis. *Nat. Methods*, 10.1038/nmeth.2019.
79. Dame,R.T., Noom,M.C. and Wuite,G.J.L. (2006) Bacterial chromatin organization by H-NS protein unravelled using dual DNA manipulation. *Nature*, 10.1038/nature05283.
80. Di Paolo,D., Afanzar,O., Armitage,J.P. and Berry,R.M. (2016) Single-molecule imaging of electroporated dye-labelled chey in live escherichia coli. *Philos. Trans. R. Soc. B Biol. Sci.*, **371**.
81. Nenninger,A., Mastroianni,G. and Mullineaux,C.W. (2010) Size dependence of protein diffusion in the cytoplasm of Escherichia coli. *J. Bacteriol.*, 10.1128/JB.00284-10.
82. Scott,M.S., Boisvert,F.M., McDowall,M.D., Lamond,A.I. and Barton,G.J. (2010) Characterization and prediction of protein nucleolar localization sequences. *Nucleic Acids Res.*, 10.1093/nar/gkq653.
83. Scott,M.S., Troshin,P. V. and Barton,G.J. (2011) NoD: A Nucleolar localization sequence detector for eukaryotic and viral proteins. *BMC Bioinformatics*, 10.1186/1471-2105-12-317.
84. Martin,R.M., Ter-Avetisyan,G., Herce,H.D., Ludwig,A.K., Lättig-Tünnemann,G. and Cardoso,M.C.

(2015) Principles of protein targeting to the nucleolus. *Nucleus*, 10.1080/19491034.2015.1079680.
85. Goedhart,J., Von Stetten,D., Noirclerc-Savoye,M., Lelimousin,M., Joosen,L., Hink,M.A., Van Weeren,L., Gadella,T.W.J. and Royant,A. (2012) Structure-guided evolution of cyan fluorescent proteins towards a quantum yield of 93%. *Nat. Commun.*, 10.1038/ncomms1738.
86. Musinova,Y.R., Lisitsyna,O.M., Golyshev,S.A., Tuzhikov,A.I., Polyakov,V.Y. and Sheval,E. V. (2011) Nucleolar localization/retention signal is responsible for transient accumulation of histone H2B in the nucleolus through electrostatic interactions. *Biochim. Biophys. Acta - Mol. Cell Res.*, 10.1016/j.bbamcr.2010.11.003.
87. Kawakami,K. (2005) Transposon tools and methods in zebrafish. *Dev. Dyn.*, 10.1002/dvdy.20516.
88. Kawakami,K. (2007) Tol2: A versatile gene transfer vector in vertebrates. *Genome Biol.*, 10.1186/gb-2007-8-s1-s7.
89. Guzman,L.M., Belin,D., Carson,M.J. and Beckwith,J. (1995) Tight regulation, modulation, and high-level expression by vectors containing the arabinose P(BAD) promoter. *J. Bacteriol.*, 10.1128/jb.177.14.4121-4130.1995.
90. Zhang,M., Chang,H., Zhang,Y., Yu,J., Wu,L., Ji,W., Chen,J., Liu,B., Lu,J., Liu,Y., *et al.* (2012) Rational design of true monomeric and bright photoactivatable fluorescent proteins. *Nat. Methods*, 10.1038/nmeth.2021.
91. Lau,I.F., Filipe,S.R., Søballe,B., Økstad,O.A., Barre,F.X. and Sherratt,D.J. (2003) Spatial and temporal organization of replicating Escherichia coli chromosomes. *Mol. Microbiol.*, 10.1046/j.1365-2958.2003.03640.x.
92. Bindels,D.S., Haarbosch,L., Van Weeren,L., Postma,M., Wiese,K.E., Mastop,M., Aumonier,S., Gotthard,G., Royant,A., Hink,M.A., *et al.* (2016) MScarlet: A bright monomeric red fluorescent protein for cellular imaging. *Nat. Methods*, 10.1038/nmeth.4074.
93. Chertkova,A.O., Mastop,M., Postma,M., Bommel,N. van, Niet,S. van der, Batenburg,K.L., Joosen,L., Gadella,T.W.J., Okada,Y. and Goedhart,J. (2017) Robust and Bright Genetically Encoded Fluorescent Markers for Highlighting Structures and Compartments in Mammalian Cells. *bioRxiv*, 10.1101/160374.

Supplementary Information

Supplementary methods:

Cloning HI-NESS overproduction vectors:

For protein overproduction, the HI-NESS gene encoding an N-terminal His-tag and a TEV-cleavable linker was cloned into a pET28a vector using Gibson Assembly (70). The plasmid was checked by Sanger sequencing and archived in a DH5α glycerol stock.

HI-NESS overproduction and purification

Plasmid pRD421 for the expression of N-terminally His-tagged HI-NESS with a TEV cleavable linker was transformed into BL21 (DE3) pLysS cells. 5 mL of an overnight culture of a single colony was used to inoculate 500 mL of LB medium. The culture was grown at 37 °C to an OD_{600} of 0.2 and thereafter, induced for 6 hours with 1 mM IPTG. The cells were pelleted by centrifugation and resuspended in 10 mL of low-salt binding buffer (130 mM NaCl, 20 mM Tris, 10% glycerol, 8 mM β-mercaptoethanol, and 3 mM benzamidine, pH 7.2) with 1 µg/mL DNase, 100 µg/mL lysozyme, and 1 mM PMSF. The cells were lysed by sonication and the soluble fraction was loaded on a 1 mL HisTrap™ HP column (Amersham Biosciences). The column was washed with 5 mL of high-salt binding buffer (500 mM NaCl, 20 mM Tris, 10% glycerol, 8 mM β-mercaptoethanol, and 3 mM benzamidine, pH 7.2) and, subsequently, His-tagged HI-NESS was eluted with 100% elution buffer (130 mM NaCl, 20 mM Tris, 10% glycerol, 8 mM β-mercaptoethanol, 3 mM benzamidine, and 500 mM Imidazole, pH 7.2). The peak fractions were exchanged back to low-salt binding buffer with a PD-10 Desalting column (Amersham Biosciences). The protein was cleaved for 48 hours at 4°C with 1 mg of TEV in the low-salt buffer supplemented with 10 mM DTT, and 2 mM EDTA to produce HI-NESS with a single glycine scar at the N-terminal. The cleavage reaction was loaded on a 1 mL HisTrap™ HP column (Amersham Biosciences) and washed with high-salt binding buffer to elute HI-NESS. HI-NESS was immediately exchanged to low-salt binding buffer with a PD-10 Desalting column (Amersham Biosciences). Protein concentration was determined using the Molar extinction co-efficient of mEos3.2 at 507 nm. 10 µL aliquots of the protein were flash-frozen in liquid nitrogen and stored at -80 °C until use.

Electrophoretic mobility shift assay

Purified HI-NESS was serially diluted in low-salt binding buffer (130 mM NaCl, 20 mM Tris, 10% glycerol, 8 mM β-mercaptoethanol, and 3 mM benzamidine, pH

7.2). The dilutions were mixed with an equivalent volume of 1 µM AT- or GC-rich DNA or RNA (Table S4.2) in nucleic acid buffer (10 mM Tris, 1 mM EDTA, and 50 mM NaCl, pH 7.5) and incubated for 20 minutes at 25 °C followed by 10 minutes at 4 °C. The samples were resolved on a polyacrylamide gel (Mini-Protean® TGX™ precast gels, 4-15%, Bio-Rad) at 30 V at 4 °C. Experiments were performed in triplicate. The polyacrylamide gels were stained for 45 minutes in a solution of 10X GelRed (Biotium) and thereafter imaged with GelDoc™ XR+ (Bio-Rad) using Bio-Rad's ImageLab software. The 'Plot profile' function in Fiji was used to quantify the unbound nucleic acid for each HI-NESS dilution. The percentage of bound nucleic acid was calculated therefrom. The dissociation constant (Kd) of HI-NESS for AT- and GC-rich DNA and RNA was extracted from a non-linear fit of the binding curves assuming specific binding with a Hill slope using the Prism8 software.

Supplementary figures:

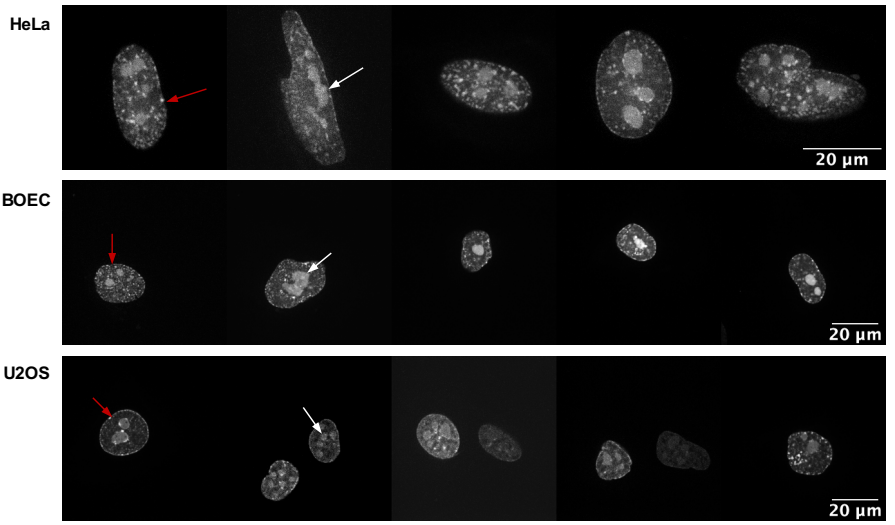

Figure S4.1: HI-NESS labels chromosomes in eukaryotic cells in culture. The HI-NESS signal appears as discrete and dense foci in nuclei (red arrows) and accumulates in nucleoli (white arrows).

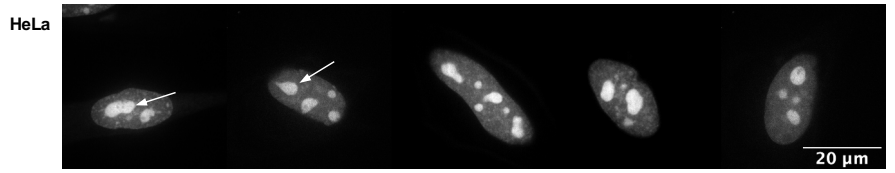

Figure S4.2: NLS-mEos3.2-NLS accumulates in the nucleoli. The mEos3.2 signal in HeLa cells expressing NLS-mEos3.2-NLS is observed primarily in the nucleoli (white arrows). The nuclei do not exhibit the distinct 'speckled' pattern that is observed when the chromosomes are stained with HI-NESS or SiR-Hoechst (Figure 4.2 and S4.1).

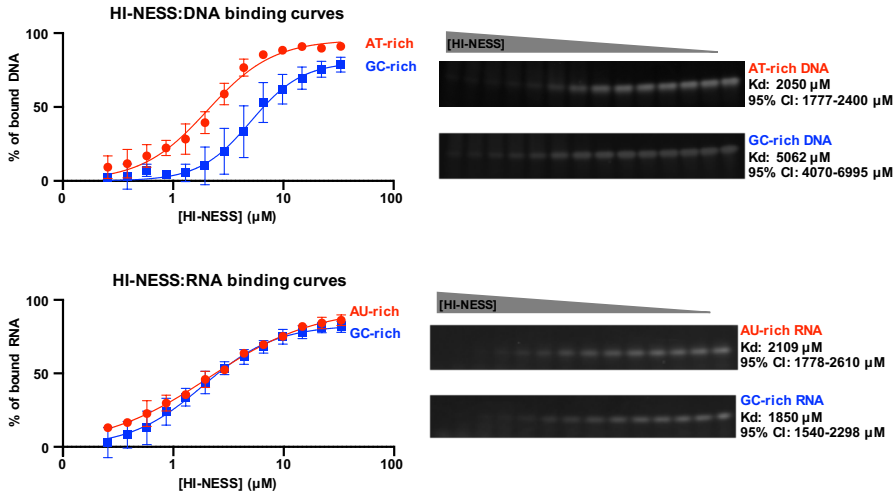

Figure S4.3: *In vitro* binding affinities of HI-NESS for DNA and RNA. The binding affinities of HI-NESS for AT/AU- and GC-rich DNA and RNA were estimated using an electrophoretic mobility shift assay (see supplementary methods). Representative results are shown on the right panel. **AT-rich DNA:** Kd = 2050 μM, 95% CI = 1777-2400 μM; **GC-rich DNA:** Kd = 5062 μM, 95% CI = 4070-6995 μM; **AU-rich RNA:** Kd = 2109 μM, 95% CI = 1778-2610 μM; **GC-rich RNA:** Kd = 1850 μM, 95% CI = 1540-2298 μM. HI-NESS displays a high affinity for RNA *in vitro*, however, the scarce nucleolar accumulation of HI-NESS in cells of zebrafish larvae (Figure S4.5; Movies S4.1-S4.5, S4.10) indicate that this affinity does not extrapolate *in vivo*.

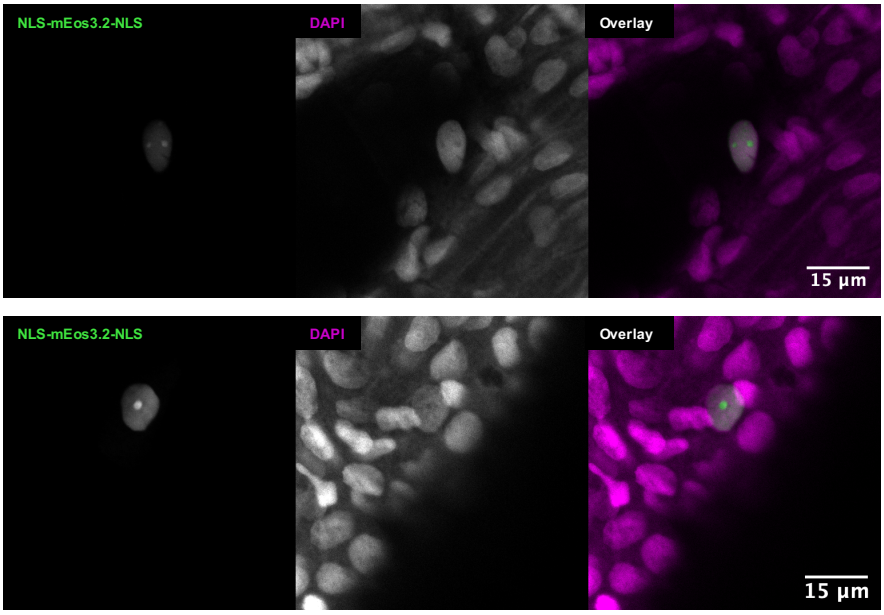

Figure S4.4: NLS-mEos3.2-NLS (green) does not recapitulate the distribution of DAPI (magenta) in nuclei of zebrafish larvae.

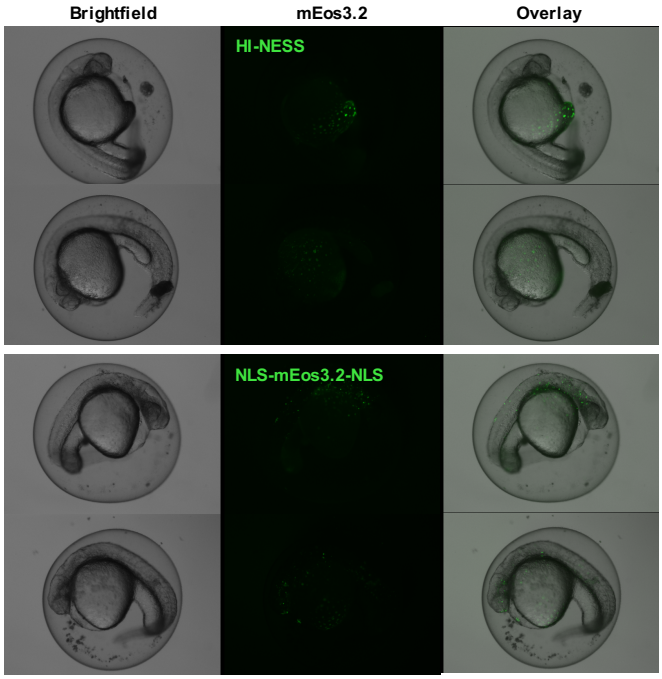

Figure S4.5: The mosaic expression of HI-NESS and NLS-mEos3.2-NLS in zebrafish larvae.

Supplementary tables:

Table S4.1:List of plasmids used in this study

Plasmid	Plasmid backbone	Insert	Resistance marker	Reference
pBAD33	pBAD33	N/A	Chloramphenicol	(89)
pcDNA3.1(+)	pcDNA3.1(+)	N/A	Ampicillin; Neomycin	Invitrogen
pRD128	pBAD33	mTurquoise2_H-NSdbd	Chloramphenicol	This chapter
pRD129	pBAD33	mEos3.2_H-NSdbd	Chloramphenicol	This chapter
pRD188	pcDNA3.1(+)	NLS_mEos3.2_H-NSdbd_NLS	Ampicillin; Neomycin	This chapter
pRD190	pcDNA3.1(+)	NLS_mEos3.2_NLS	Ampicillin; Neomycin	This chapter
pRD198*	pBAD33	mEGFP_H-NSdbd	Chloramphenicol	This chapter
pRD395*	pBAD33	mCherry_H-NSdbd	Chloramphenicol	This chapter
pRD396	pBAD33	eYFP_H-NSdbd	Chloramphenicol	This chapter
pRD397	pcDNA3.1(+)	NLS_mTurquoise2_H-NSdbd_NLS	Ampicillin; Neomycin	This chapter
pRD398*	pcDNA3.1(+)	NLS_mCherry_H-NSdbd_NLS	Ampicillin; Neomycin	This chapter
pRD399*	pcDNA3.1(+)	NLS_mEGFP_H-NSdbd_NLS	Ampicillin; Neomycin	This chapter
pRD400	pcDNA3.1(+)	NLS_eYFP_H-NSdbd_NLS	Ampicillin; Neomycin	This chapter
pRD403	pBAD33	mScarlet-I_H-NSdbd	Chloramphenicol	This chapter
pRD404	pBAD33	mNeonGreen_H-NSdbd	Chloramphenicol	This chapter
pRD405	pcDNA3.1(+)	NLS_mScarlet-I_H-NSdbd_NLS	Ampicillin; Neomycin	This chapter
pRD406	pcDNA3.1(+)	NLS_mNeonGreen_H-NSdbd_NLS	Ampicillin; Neomycin	This chapter
pRD421	pET28a	His-tag_TEV-cleavable linker_mEos3.2_H-NSdbd	Kanamycin	This chapter
pmTurquoise2_C1	pEGFP-C1	mTurquoise2	Kanamycin; Neomycin	(85)
mEos3.2-C1	mEos3.2-C1	mEos3.2	Kanamycin; Neomycin	Addgene #54550 (90)
pLau53	pBAD24	eYFP	Ampicillin	(91)
pmScarlet-i_C1	pC1	mScarlet-I	Kanamycin	From TWJG Addgene #85044 (92)
LifeAct-mNeonGreen	pEGFP-N1	mNeonGreen	Kanamycin	From TWJG Addgene #98877 (93)

* Sequences for mCherry, and mEGFP were prepared with PCR and Gibson assembly.

Table S4.2: List of nucleic acids (Sigma-Aldrich) used for the electrophoretic mobility shift assays.

Nucleic acid	Sequence
AT-rich dsDNA	5'-ATGGCAATTAAATTAGAAATTAAAAATCTTTATAAAATATTTGGC-3'
GC-rich dsDNA	5'-ATGGCAATCAAACTCGAGATCAAGAACCTCTACAAGATCTTCGGC-3'
AU-rich ssRNA	5'-AUGGCAAUUAAAUUAGAAAUUAAAAAUCUUUAUAAAAUAUUUGGC-3'
GC-rich ssRNA	5'-AUGGCAAUCAAACUCGAGAUCAAGAACCUCUACAAGAUCUUCGGC-3'

Supplementary movies:
Movies S4.1-S4.10 are available in the attached electronic supplement:
2021_Rashid_PhD_Thesis/Electronic_Supplement/Chapter 4/

Movies S4.1-S4.5: HI-NESS labels chromosomes in Zebrafish larvae. The distribution of the mEos3.2 signal (green) in nuclei of zebrafish larvae overlapped with that of DAPI (magenta). Nucleolar accumulation of HI-NESS was not observed. **S4.1:** Epithelial cells (tail fin); **S4.2:** Muscle cells (trunk); **S4.3:** Yolk syncytial cells (yolk syncytial layer); **S4.4:** From left to right: trunk, blood vessel, yolk extension; **S4.5:** Yolk syncytial cells (yolk syncytial layer).

Movies S4.6-S4.8: NLS-mEos3.2-NLS does not label the chromosomes in zebrafish larvae. In cells of zebrafish larvae expressing NLS-mEos3.2-NLS (green), the fluorophore accumulates in nucleoli and distributes uniformly over the non-nucleolar regions of the nucleus. The distribution does not correlate with that of DAPI (magenta). **S4.6:** Muscle cells (trunk); **S4.7:** Left: muscle cells (trunk), right: epithelial cells (skin); **S4.8:** Yolk syncytial cells (yolk syncytial layer).

Movie S4.9: HI-NESS can be used to follow chromosome dynamics in eukaryotic cells in culture. The time-lapse (in min:sec) shows cell division in a HeLa cell. From left to right: Phase contrast image, Lck-mTurquoise2 membrane label, HI-NESS (mScarlet-I).

Movie S4.10: HI-NESS (mScarlet-I) can be used to follow the movements of nuclei in a live animal model.